SCIREA Journal of Electrical Engineering

http://www.scirea.org/journal/DEE

December 3, 2020

Volume 5, Issue 6, December 2020

Temperature and magnetic field dependence of the specific heat of van der Waals gapped ferromagnet CrI_3

K. Spurgeon[1], G. Kozlowski[1,2,3], M.A. Susner[2,3], Z. Turgut[2], J. Boeckl[2]

[1]Physics Department, Wright State University, Dayton, Ohio 45435, USA

[2]AFRL, Wright Patterson AFB, Dayton, Ohio 45433, USA

[3]UES Inc., 4401 Dayton Xenia Rd, Dayton, Ohio 45432, USA

Abstract

Chromium (III) iodide (CrI_3) is a layered 2-D semiconducting magnet in which strong ferromagnetic order is present within individual layers with possibly weak magnetic coupling between them. In this report we study the specific heat of this interesting compound as functions of both temperature and magnetic field. The layered structure of this material suggests that the specific heat may be theoretically described by either the two- or three-dimensional models. Here we evaluate each model in terms of comparison to experimental data taken on single crystals. It appears that the specific heat capacity of CrI_3 is well described by the combination of a structural (phonon) 3-D contribution and a 2-D magnetic contribution. Spin wave theory applied to describe 2-D magnetic contribution to specific heat capacity in the low temperature region shows the presence of a very strong anisotropy which is required to keep magnetic moments in an off-plane orientation.

Keywords: 2-D semiconducting magnet, heat capacity

I. INTRODUCTION

A strong magnetic anisotropy is one of the critical requirements to establish 2-D magnetism in a system. In some ultrathin metallic films, an easy anisotropy axis can originate from symmetry reduction at the interface between the film and the substrate. A similar situation is created in CrI_3, a 2-D van der Waals gapped magnet where an intrinsic magneto-crystalline anisotropy is created due to the reduced crystal symmetry in the layered structure. Recent work has shown that CrI_3, when exfoliated to the monolayer, retains magnetic order[1], a feature useful for device fabrication[2,3].

CrI_3 is a 2-D van der Waals gapped structure which exhibits coupled structural and magnetic phase transitions[4]. The structure crystallizes at reaction temperatures of 650°C into the monoclinic $C2/m$ $AlCl_3$-type space group. At ~ 215 K the structure transforms into a rhombohedral structure ($R\bar{3}$). Ferromagnetism, with spins pointed along the c direction (see, Fig.1), emerge at 61 K in bulk crystals and has been shown to persist down to the monolayer with only a slight degradation in T_C (45 K)[5].

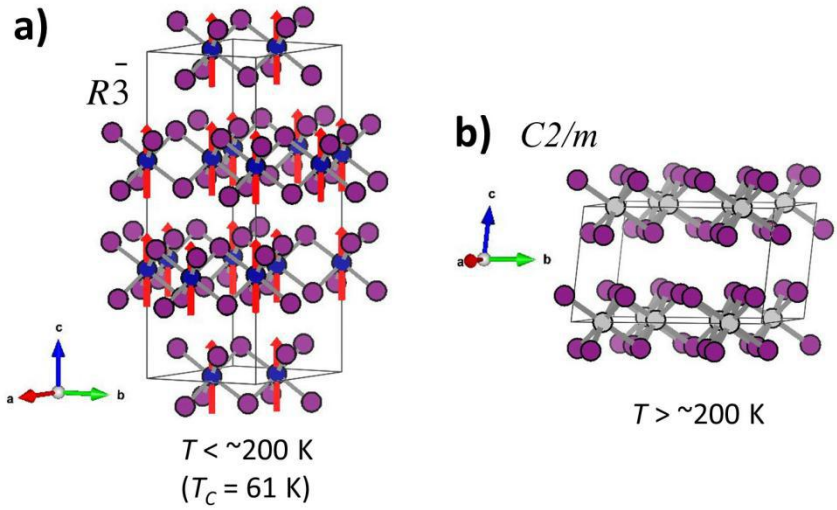

FIG. 1. Crystal structure of CrI_3 below (a) and above (b) the structural transition temperature T_S ~ 200 K.

Chromium trihalides CrX_3 (X = Cl, Br, I) are class of van der Waals (vdW) bonded, magnetic layered semiconductors important for spintronic and magnetoelectronic applications[6–9]. As a cleavable single crystal, they are especially an attractive as monolayer or as a few layers in terms of applications. The Cr^{3+} ions are in a hexagonal arrangement with each cation located in the center of edge sharing octahedra circumscribed by X^- anions. The shared edges of the octahedra are responsible for the exchange interaction between two Cr atoms (Cr – X – Cr).

The resulting layers of CrX_3 are stacked, with offsets determined by the specific symmetry of the structural phase, via van der Waals bonded layers. The compounds adopt monoclinic or rhombohedral crystallographic structures, as shown in Table I together with a summary of magnetic (T_C and T_N) and structural (T_S) phase transition temperatures in CrX_3 crystals and summaries of the type of magnetic ordering.

TABLE I. Partial magnetic and structural properties of chromium trihalides.

	Magnetic Transition	Structural Transition	Magnetic Moment	Magnetic Order	vdW gap (nm)
$Cr Cl_3$	T_N = 17 K	T_S = 240 K	m ∥ layer	AF/F	0.2698
$Cr Br_3$	T_C = 37 K	T_S = 420 K	m ⊥ layer	F	0.2909
$Cr I_3$	T_C = 68 K	T_S = 210 K	m ⊥ layer	F	0.3174

Our study concentrates on CrI_3. It has been reported (Tab. I) that among chromium trihalides, CrI_3 has the highest bulk T_C at 68 K, the strongest effective anisotropy with a magnetic moment perpendicular to the CrI_3 planes and is the easiest to cleave for device fabrication. McGuire *et al.*[4] discussed the correlation between magnetic and crystallographic properties of CrI_3 single crystals and demonstrated the existence of the magnetoelastic coupling between magnetic and structural properties. The high-temperature monoclinic and low-temperature rhombohedral structures of CrI_3 is characterized by a change in the layer spacing from d = 0.6623 nm to d = 0.6602 nm, respectively. It takes place at T_S = 210 K as a first-order crystallographic phase transition. Near a magnetic phase transition of T_C = 61 K, a presence of the long-range order of the ferromagnetic phase is evidenced via the enhanced thermal expansion along the stacking direction, suggesting a small anomaly/contraction in the layer spacing of the crystallographic lattice. In Table II we summarize the magnetic parameters of T_C, saturation moment (m_s), and Weiss temperature ( ) of CrI_3 for both materials derived from powder synthesis[10-12] and for the single crystal work performed by McGuire *et al.*[4].

TABLE II. Curie temperature (T_C), saturation moment (m_S), and Weiss temperature (θ) for BrI_3.

	T_C(K)	$m_S(\mu_B)$/Cr	θ(K)
Dillon/Olson (powder) [12]	68	3.10	70
McGuire et al. (crystal) [4]	61	3.10	72

Previous specific heat capacity measurements of CrI_3 crystals[4] showed 1) a clear lambda-type anomaly at T_C, 2) the Curie-Weiss behavior due to magnetic correlations prevail up to approximately $2T_C$, and 3) confirmation of the Delong-Petit value at high temperatures (C_P = R ln(2S+1) for S = 3/2, Cr^{3+}). Low-temperature behavior of the specific heat capacity[4] shows a linear term in *T* due to magnetic excitations associated with 2-D ferromagnetic nature of CrI_3[13] in addition to the phonon contribution T^3. By comparing theoretical and experimental data to match relationship $C_P/T = 0.00117 + 9.8x10^{-5}\ T^2$, McGuire *et al.*[4] estimated the Debye temperature θ_D to be 134 K. Liu *et al.*[1] investigated the suppression of the magnetic transition temperature T_C (bulk) = 61 K with the thickness of CrI_3 crystals. It was observed also an additional transition at 45 K, independent on the thickness of the film, corresponding to T_C for monolayer of 2-D CrI_3. Lado *et al.*[14] studied theoretically the origin of off-plane, strong magnetic anisotropy in 2-D CrI_3 responsible for the orientation of a magnetic moment of Cr^{3+} ion normal to layers. Their calculations based on the electron density functional theory that include spin-orbit interactions to consider magnetic anisotropy, result in the values of an isotropic exchange coupling J = 2.2 meV, an anisotropic exchange interaction λ = 0.09 meV, and a single ion anisotropy $D \approx 0$. The effective spin Hamiltonian describing 2-D CrI_3 by Lado *et al.*[14] is an XXZ-type leading to the gapped spin waves excitations affecting the finite temperature properties of the system. Lin *et al.*[15] investigated the critical behavior of 2-D CrI_3 in the vicinity of magnetic transition T_C = 64 K by using a modified Arrott plot[16], the critical isotherm and Kouvel-Fischer method[17], and they obtained the critical exponents and concluded the presence of the crossover behavior of a 3-D Ising model with mean-field type interactions. The spontaneous magnetization just below T_C suggests that CrI_3 possesses 3-D Ising behavior in contrast to the inverse initial susceptibility just above T_C and the magnetization at T_C which indicates mean field interactions. In addition, Lin *et al.*[15] have shown that the experimental specific heat capacity data as a function of temperature in the vicinity of second order phase transition (the lambda-type anomaly at T_C) is close to 3-D Ising behavior[18]. Based on existing results, one of the interesting aspects of the bulk properties of CrI_3 is the fact that despite 2-D structural characteristics with a large van der Waals gap (vdW, see Tab. I), the small cleavage energy[19,20], and the strong magnetic anisotropy[4-5,14,21-22], there are distinct 3-D magnetic properties, at least in the vicinity of transition temperature[15]. A main goal of our research is a first to measure the specific heat capacity of CrI_3 bulk single crystal in the range of temperature from 2 K to 200 K and in the presence of the external magnetic field up to 5 T applied normal to the stacking direction to determine the degree of 2D and/or 3D phonon and magnon contributions. The spin wave

approximation valid at temperatures below T_C allows one to find analytically magnetic contribution for 2-D or 3-D CrI_3 system.

II. EXPERIMENTAL METHODS

CrI_3 crystals were grown by the vapor transport method using a reaction of the reduced Cr powder (99.999%) with anhydrous I_2 (99.999%)[4]. The ratio of Cr and I was stoichiometric. The powders were sealed inside of a thick-walled (2mm) quartz ampoule of 14 cm length. The ampoule was placed inside of a tube furnace with a temperature at the center of 650°C (after a slow ramp up of 20°C/hr.). The tube was arranged in such a way the hot end experienced a temperature of 650°C and the cold end saw a temperature of 560°C. The sample was kept at temperature for 10 days, after which the tube furnace was slowly cooled to room temperature. The extracted CrI_3 crystals varied in size from the microscopic to ~1x1 cm^2 in size, grew as platelets along the *ab* plane, and were micaceous in nature. Care was taken to store the material in the absence of moisture, which has been shown to chemically degrade the compound[23].

The powder X-ray diffraction off of a crystal surface was performed by using a Bruker D8 Discover DaVinci system outfitted with a Co anode (Co K = 1.79026 Å) (see, Fig.2). The diffraction data were fit using a LeBail fitting with the monoclinic angle artificially fixed to 90° so as to obtain a layer thickness of 6.63299(11) Å (where one layer represents the sum of one lamella and one van der Waals gap).

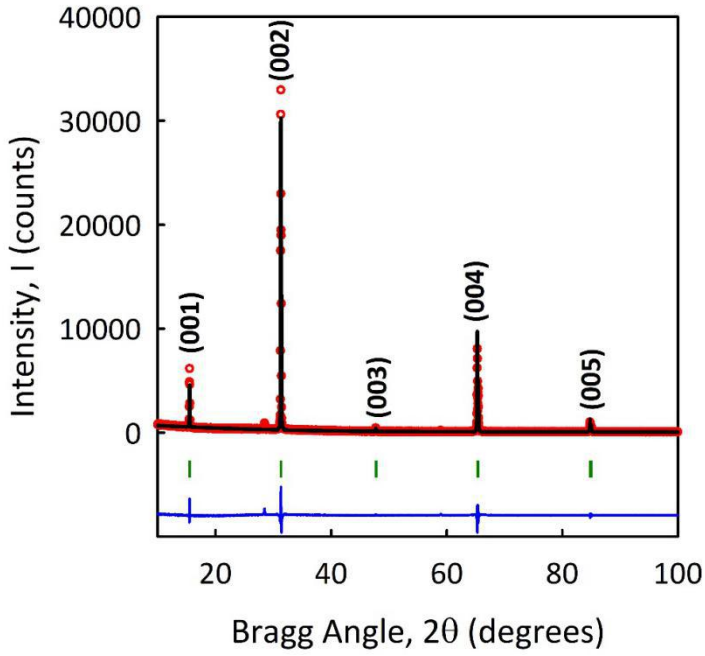

FIG. 2. Powder XRD pattern of crystal surface taken with Co K radiation, = 1.79026 Å.

Specific heat measurements were performed using the heat capacity option on a 9 T Quantum Design Physical Property Measurement System (PPMS). This technique uses the pulsed calorimetry technique whereby a small amount of thermal energy is imparted to the sample and the temperature decay over a period of time is recorded and fitted to Eq. (1)

$$C_{TOTAL}\,(dT/dt) = -K_W\,(T - T_B) + P(t) \qquad (1)$$

where C_{TOTAL} is the total heat capacity (sample, fixture grease, and sample platform), K_w is the thermal conductance of the support wires, T_B is the base temperature (i.e. of the system), and P(t) is the applied heater power (equal to P_0 during heating and 0 afterward). The specific heat of the sample itself was isolated by us first performing the measurement on the sample holder with only the fixture grease (Apiezon N) and then subtracting these measurements from those performed with the sample included. After achieving a base temperature of 2 K, samples were gradually increased in temperature with three measurements taking place at each temperature setpoint. We performed measurements in external magnetic fields (H = 0 T, 2 T, 4 T, 5 T, and 9 T) applied along the c-axis of the CrI_3 crystal (Fig.3a, b).

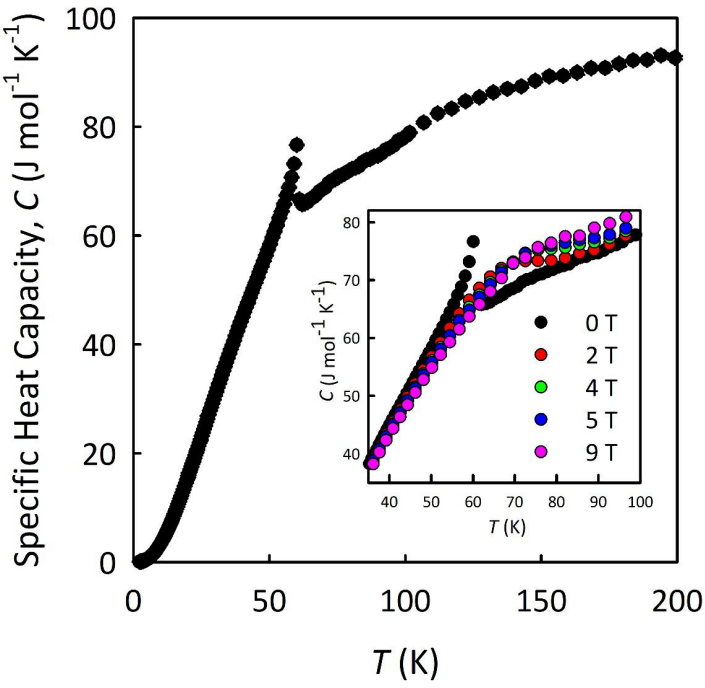

FIG. 3a. Specific heat capacity C of CrI_3 from T = 2 K to T = 200 K for H = 0 T. Inset: specific heat capacity C of CrI_3 from T = 2 K to T = 100 K in the external magnetic fields H = 0 T, 2 T, 4 T, 5 T, and 9 T.

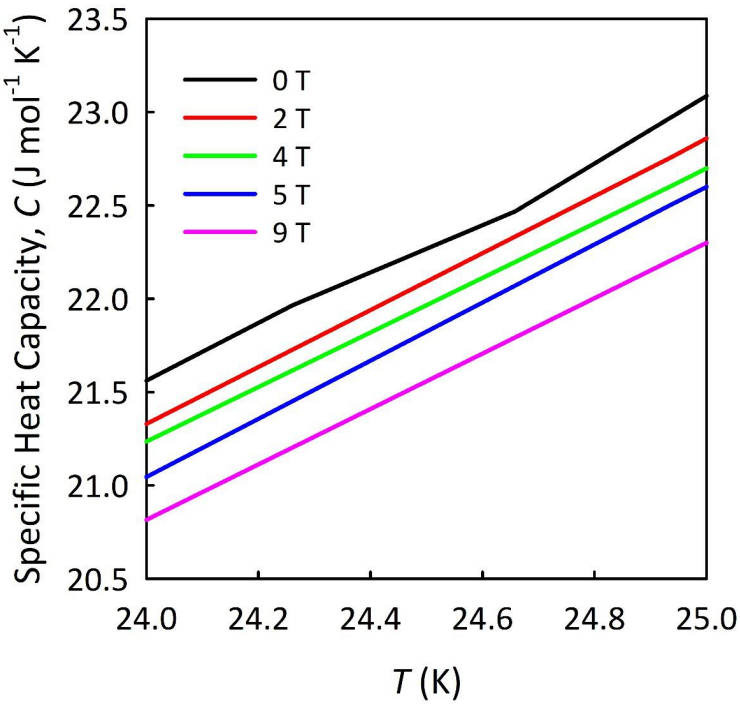

FIG. 3b. Specific heat capacity C of CrI_3 in the external magnetic field H = 0 T, 2 T, 4 T, 5 T, and 9 T applied parallel to c-axis from 24 K to 25 K.

III. THEORETICAL CONSIDERATIONS

Specific heat capacity of magnetic materials usually has three main contributions. First the phonon contribution comes from lattice vibration. Second is the electronic contribution due to the presence of free electrons in the material, which would obviously be diminished in a semiconducting material. The third contribution is due to presence of magnetic moments with ferromagnetic order below the Curie temperature T_C and paramagnetic order above it. Magnetic contributions to specific heat capacity are difficult to calculate analytically in the entire range of the ferromagnetic phase. Until now, there is no physical model that can described magnetic contribution with desired accuracy. Our effort will concentrate only on the low-temperature approximation ($T < T_C$) where we can use the spin-wave approach to find magnetic contribution under assumption that magnon-magnon interaction is negligible.

A. The 3-D model

The 3-D phonon portion of heat capacity can be found by using the Debye model which requires one to know the thermal energy U (Eq.(2)) of the system, the density of states D(ω) (Eq.(3)), the average thermal equilibrium occupancy of the phonons <n(ω)>, the angular frequency of the phonons ω, the velocity of sound v_S, and the volume V of the system[24],

$$U = \int d\omega\, D(\omega) \langle n(\omega) \rangle \hbar\omega \qquad (2)$$

$$D_{3\text{-}D}(\omega) = V\, \omega^2 / 2\, \pi^2\, v_S{}^3 \qquad (3)$$

By substituting the density of states (Eq.(3)) into the thermal energy (Eq.(2)) and differentiating with respect to temperature we can find the specific heat capacity due to phonons in the entire range of temperatures (Eqs.(4) and (5)),

$$C = dU/dT \qquad (4)$$

$$C_{ph} = 9\, N\, k_B \left(\frac{T}{\theta_D}\right)^3 \int_0^{\theta_D/T} \frac{x^4 e^x}{(e^x-1)^2} dx \qquad (5)$$

where N is the number of lattice points per unit volume, k_B is Boltzmann's constant, and θ_D is the Debye temperature[24,25]. For low temperature approximation, a phonon contribution of the specific heat capacity (Eq. (5)) leads to the following version of C_{ph} (Eq.(6)) for 3-D,

$$C_{ph} = C_{3\text{-}D} = 234\, N\, k_B\, (T/\theta_D)^3 = \beta_{3\text{-}D} T^3 \qquad (6)$$

where $\beta_{3\text{-}D}$ is a proportionality constant which depends on Debye temperature θ_D.

To find the electron contribution to the specific heat capacity (C_{el}), we assume the available free electrons (conduction electrons) in the ferromagnetic semiconductor CrI_3 scale linearly with temperature following the relation:

$$C_{el} = \gamma_{3\text{-}D}\, T \qquad (7)$$

where the constant γ is known as the Sommerfeld coefficient[24].

The magnetic contribution to the specific heat capacity in a 3-D ferromagnet using the spin wave (magnon) approximation at the low temperature range is represented by:

$$C_{mag} = A_{3\text{-}D}\, T^{3/2} \qquad (8)$$

with a coefficient $A_{3\text{-}D}$ called the spin wave stiffness constant [24]. Combining together Eqs. (6), (7), and (8), the total 3-D specific heat capacity (Eq. (9)) in the low-temperature regime is given by:

$$C_{total} = C = C_{3\text{-}D} = \beta_{3\text{-}D}T^3 + \gamma_{3\text{-}D}T + A_{3\text{-}D}T^{3/2} \qquad (9)$$

B. The 2-D model

For two-dimensional ferromagnetic system (2-D), at least three contributions are present; phonon, electron, and magnon. The same method as above (Eqs. (2) and (4)) are used to determine the specific heat capacity due to phonons with 2-D density of states described by Eq. (10). In the entire temperature range, the specific heat capacity is described by Eq. (11), and in the limit of the low temperature approximation, it leads to Eq. (12)[7],

$$D_{2\text{-}D}(\omega) = A\, \omega / 2\pi v_S^2 \qquad (10)$$

$$C_{ph} = 3\, N\, k_B \left(\frac{T}{\theta_D}\right)^2 \int_0^{\theta_D/T} \frac{x^3 e^x}{(e^x-1)^2}\, dx \qquad (11)$$

$$C_{ph} = C_{2\text{-}D} = 24\, N\, k_B\, (T/\theta_D)^2 = \beta_{2\text{-}D}T^2 \qquad (12)$$

where A is the area of the unit cell.

The electronic contribution to the heat capacity is also linear in two dimensions; however, the Sommerfeld coefficient $_{2\text{-}D}$ has a different value[25]:

$$C_{el} = \gamma_{2\text{-}D}\, T \qquad (13)$$

The magnetic contribution to specific heat capacity, using the spin wave approximation in the low temperature regime, reduces to[14]:

$$C_{mag} = C_{2\text{-}D} = (B\alpha/2)\, [2 + \alpha T^{-1} + 2T\alpha^{-1}] \exp(-\alpha/T) \qquad (14)$$

$$\alpha = (K_{eff} + g\,\mu_B\,H)/k_B \qquad (15)$$

where α is a parameter in units of Kelvin that is dependent on the externally applied magnetic field H (Eq. (15)), g is the Landé g-factor, μ_B is the Bohr magneton, K_{eff} is an effective anisotropy constant, and B = 2/3. At very low temperatures ($\alpha/T >> 0$) the following term

$$C_{mag} = (B\alpha^2/2T)\exp(-\alpha/T) \qquad (16)$$

dominates but when $\alpha/T < 1$ is quickly overtaken by the linear term reducing Eq. (14) further to:

$$C_{mag} = B\,T \qquad (17)$$

where B is a constant from Eq. (14).

It has been reported [26] that in the chromium halides and other semiconducting layered ferromagnets with antiferromagnetic ordering[27], the specific heat capacity has a linear dependence on temperature (Eq. (17)). Eqs. (16), and (17) are valid in the low temperature range and are related to the magnetic (spin wave) contribution to the specific heat capacity. Establishing the global temperature dependence of the magnetic contribution to the specific heat capacity is an intractable problem due to lack of physical model with the desired precision. Our approach simplifies the issue by simply subtracting the theoretical electron and phonon contributions described above by Eqs. (5) and (7) from experimental data.

IV. DISCUSSION OF EXPERIMENTAL RESULTS FOR SPECIFIC HEAT CAPACITY OF CrI_3

Based on Fig.3a, the heat capacity has a sharp discontinuity at T_C = 61 K which is due to the phase transition between ferromagnetic and paramagnetic order which happens at the Curie temperature T_C. Roughly at 216 K, there is another jump in heat capacity due to a shift in the geometry of the lattice when the structure transforms from the high temperature monoclinic phase to the low-temperature rhombohedral phase. Based on Figs.3a and b external magnetic field applied to the system lows the specific heat capacity at low and raises it at high temperatures (above T_C) with a crossover point at about 70 K[28].

In our physical interpretation of temperature dependence of specific heat capacity, we consider first the 3-D model in low temperature range by fitting Eqs. (6)-(9) to match to

experimental data depicted in Fig.3a. In order to find the constants in Eq. (9), namely, $\beta_{3\text{-}D}$, $\gamma_{3\text{-}D}$ and $A_{3\text{-}D}$, we split Eq. (9) into two separate equations (Eqs. (18) and (19))

$$C/T^{3/2} = \beta_{3\text{-}D}T^{3/2} + A_{3\text{-}D} \quad (18)$$

$$C/T = \beta_{3\text{-}D}T^{2} + \gamma_{3\text{-}D} \quad (19)$$

which are valid in different temperature ranges. At very low temperatures only magnon ($T << T_C$) and phonon contributions can play a role (Eq. (18)) followed by Eq. (19) at which the phonon and electron contributions is true at slightly higher temperatures.

Figs.4 and 5 represent the fitting of Eqs. (18) and (19) to experimental data in the range of temperatures between 2 K and 5 K for Eq. (18) and between 3 K to 6 K for Eq. (19).

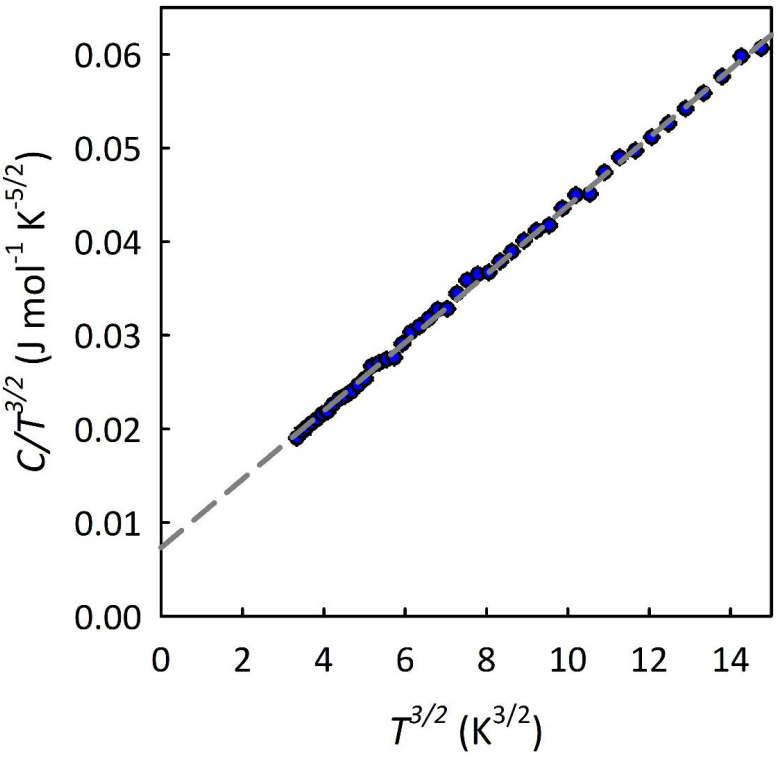

FIG. 4. Theoretical specific heat capacity (Eq. (18)) as a function of temperature fitted to experimental data in the range of temperatures between 2 K and 5 K at H = 0 T.

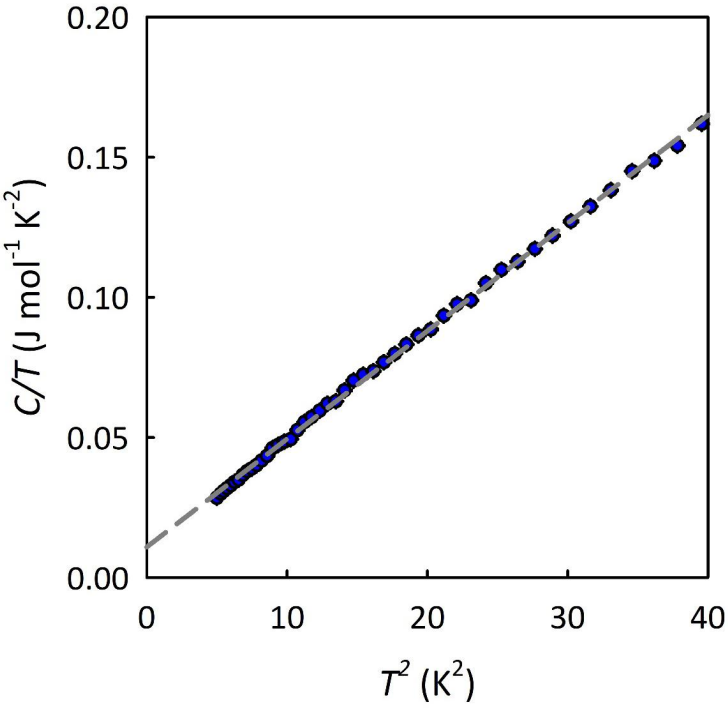

FIG. 5. Theoretical specific heat capacity (Eq. (19)) as a function of temperature fitted to experimental data in the range of temperature between 3 K and 6 K at H = 0 T.

The linear fit in Fig.4 gives $\beta_{3\text{-}D}$ = 3.651 (mJ/(mol*K^4)) and $A_{3\text{-}D}$ = 7.32 (mJ/(mol*K$^{5/2}$)) and using $\beta_{3\text{-}D}$ defined by Eq.(6), the Debye temperature Θ_D is found to be 128.7 K. Fitting in Fig.5 gives $\beta_{3\text{-}D}$ = 3.854 (mJ/(mol*K^4)) and $\gamma_{3\text{-}D}$ = 10.9 (mJ/(mol*K^2)), and the Debye temperature in this fitting is found to be 126.4 K.

For the 2-D model, Eqs. (12) and (13) are combined and then divided by T to give Eq. (20), and then a linear fit on a plot of C/T vs T can be used to find the coefficients $\beta_{2\text{-}D}$ and $\gamma_{2\text{-}D}$ (Fig.6),

$$C/T = \beta_{2\text{-}D}T + \gamma_{2\text{-}D} \qquad (20)$$

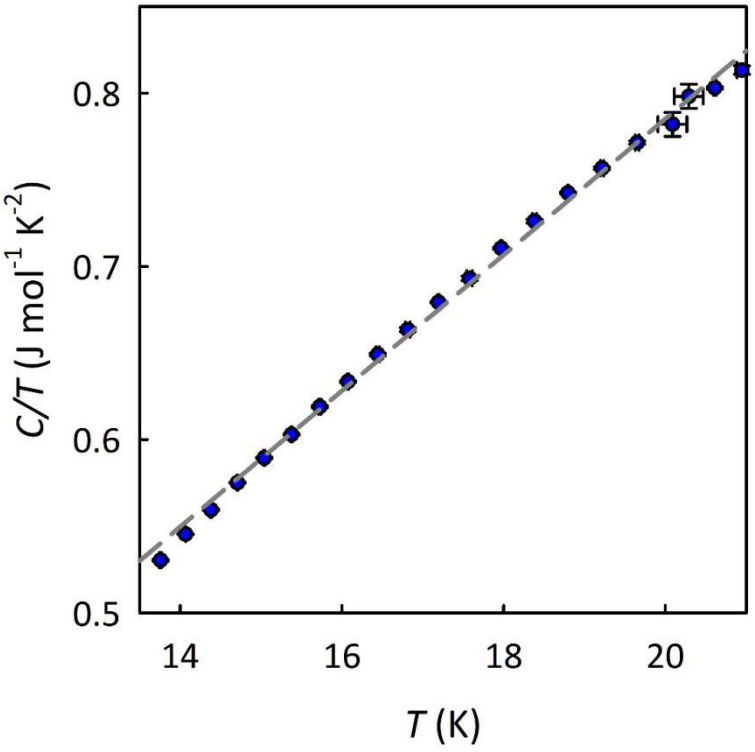

FIG. 6, Theoretical specific heat capacity (Eq. (20)) as a function of temperature fitted to experimental data in the temperature range between 14 K and 21 K at H = 0 T.

The linear fit in Fig.6 yields $\beta_{2\text{-}D}$ = 39.26 (mJ/(mol*K^3)), $\gamma_{2\text{-}D}$ = 0.0603 (mJ/(mol*K^2)), and a Debye temperature of 71.3 K. The above methods of fitting of the experimental data to the theoretical predictions were applied to low temperature regions only. It appears that the electronic contribution in the 2-D model applied to our material has a very small value for the $\gamma_{2\text{-}D}$ coefficient in contrast to the same coefficient in 3-D. However, in 3-D this linear contribution can be based on the magnetic mechanism which is due to weak coupling between layers in our system[27]. So, since our material is a semiconductor, this electronic contribution should be small in the entire range of temperature. Under these conditions the main contributions can be restricted to the phonon and magnetic mechanisms. Magnetic contributions in the entire range of temperature are difficult to quantify in contrast to phonon contribution which can be easily defined for 2-D (Eq. (11)) and 3-D (Eq. (5))[25].

From our experimental data (Fig.3a) we would like to find for CrI_3 the magnetic contribution in entire temperature range by simply subtracting theoretical values of phonon contribution of specific heat capacity (Eqs. (5) and (11)) from the experimental data (Eq. (21)),

$$C_{mag} = C - C_{ph} \qquad (21)$$

Figs.7 and 8 show the phonon contribution in 2-D and 3-D for the entire range of temperatures together with experimental data of the specific heat capacity.

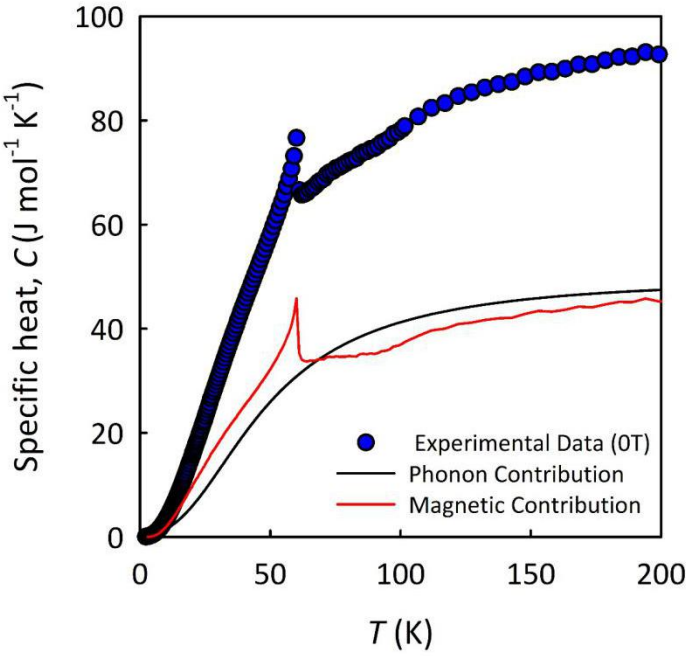

FIG. 7. Specific heat capacity as a function of temperature for the 2-D model for H = 0 T.

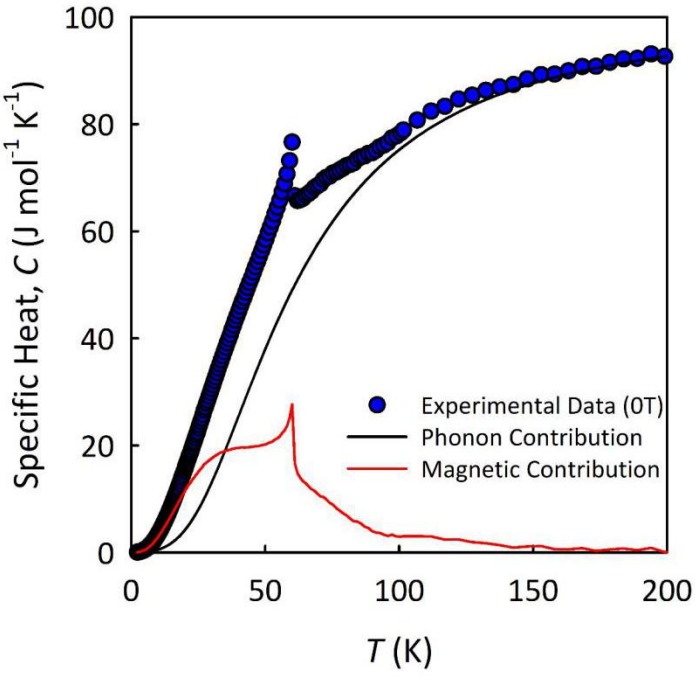

FIG. 8. Specific heat capacity as a function of temperature for the 3-D model at H = 0 T.

Subtraction of specific heat capacity data in Figs.7 and 8 from the theoretical phonon contribution allows us to see how important the magnetic contribution is in our system[15]. This analysis shows that a magnetic contribution is larger than the lattice contribution in the range

of temperature up to around 70 K in 2-D and around 40 K in 3-D. Both Figs.7 and 8 have discontinuities in specific heat capacity at the Curie temperature. In Fig.7 this is followed by a slow rise in heat capacity with increasing temperature and in Fig.8 this is followed by an exponential decay, which is the expended behavior of a paramagnetic phase.

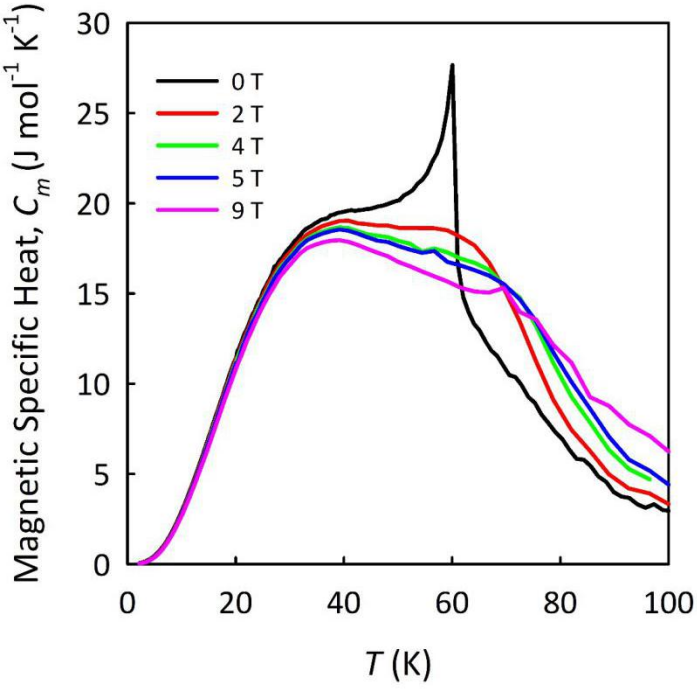

FIG. 9. Magnetic specific heat capacity vs. temperature for different values of the external magnetic fields.

The magnetic part of the specific heat capacity is higher for low values of magnetic fields at low temperature region (see, Fig.3b), in contrast to a higher temperature range where behavior follows the converse trend, namely, a higher heat capacity for high values of magnetic fields (see, Fig.9). Qualitatively, such behavior is predicted by the molecular field theory[28]. As the external magnetic field further increases, the discontinuity at the Curie temperature T_C smooths over and approaches a simple Schottky-type anomaly[28].

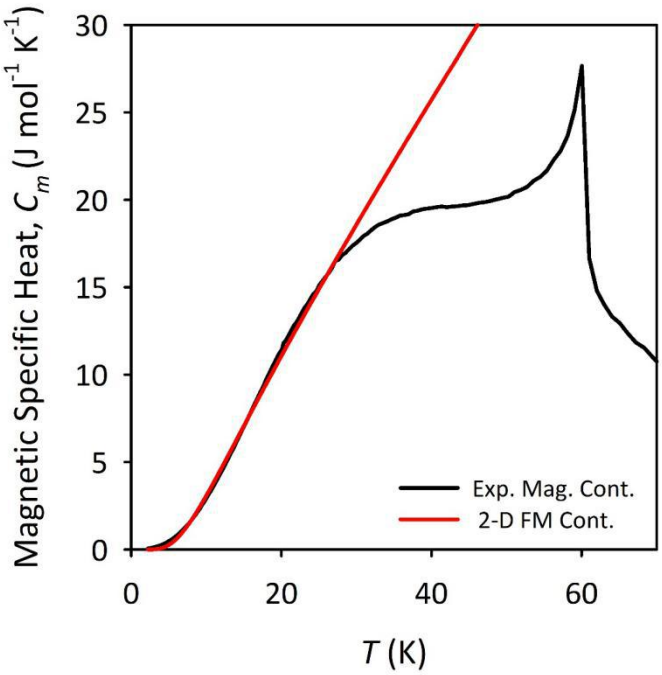

FIG. 10. Fit to the experimental data of the magnetic contribution to the specific heat capacity calculated from Eq. (14) for the range of temperature between 2 K and 20 K at H = 0 T (the theoretical low temperature approximation only for magnetic part of the specific heat capacity).

The best fit in Fig.10 between experimental magnetic specific heat capacity and theoretical 2-D ferromagnetic contribution, based on spin wave method (Eq. (14)), gives $\alpha = 28.32$ K for a temperature range of 2 K to 20 K and H = 0 T. Fig.10 shows a magnetic contribution that is slightly larger than theoretical at $T < 20$ K and that is smaller than the theoretical at high temperatures ($T > 20$ K) where the magnetic contribution begins to approach a constant value before rapidly rising into the discontinuity at the Curie temperature. A discrepancy which is present for $T > 20$ K perfectly matches to the restriction imposed on the spin wave model (no interaction between magnons) in deriving Eq. (14). Namely, the spin wave interaction must be added to this approach when temperature is roughly higher than ~ (1/3) $T_C \approx 20$ K. Other important aspects of our theoretical description of the magnetic contribution to the specific heat capacity for the 2-D CrI_3 system is to estimate magnetic parameters such as exchange interaction, anisotropy, and involvement of magnetic field intensity when compared to the experimental data (see e.g., Fig.10). The quantity B in Eq. (14) is related to the exchange interaction J in the following way (Eq. (22)[14])

$$B = N k_B^2/\pi JS \qquad (22)$$

where S = 3/2 for Cr^{3+}. The effective anisotropy constant K_{eff} in Eq. (15) incorporates a single ion anisotropy D and an exchange anisotropy λ (Eq. (23)) as follows[14]

$$K_{eff} = 2DS + 3S\lambda \qquad (23)$$

Both anisotropy constants (D and λ) favor off-plane easy axis (normal to the layers). On the other hand, due to the crystallographic symmetry of the CrI_3 crystal, single ion anisotropy is negligible (D ≈ 0). The two other parameters J and λ must be specified to compare magnetic specific heat capacity experimental data with the theoretical prediction (see Eq. (14) and Fig.10). The results of these comparisons are summarized in Tab. III. The most striking result of these calculations is the fact that for a reasonable choice of the J value (or B = 0.67 (2/3), 0.6, and 0.2) from J = 0.228 mJ to J = 0.762 mJ (Tab. III), the respective value of λ from comparison of experimental data and theoretical model ends up with a very strong anisotropy constants from 0.542 meV to 0.138 meV, respectively. This is exactly what we see in 2-D CrI_3 system where spins due to a very strong anisotropy constant are kept along the stacking direction.

TABLE III. The exchange interaction *J* and anisotropy constant *λ* established from comparison between theoretical model and experimental data for the CrI_3 crystal (Eqs. (14), (15), (22), and (23)).

B (J/mol K^2)	α (K)	J (meV)	λ (meV)	λ/J
0.67	28.32	0.228	0.542	2.38
0.60	26.52	0.254	0.508	2.00
0.20	7.23	0.762	0.138	0.18

Finally, Table IV list values of the α, γ, and A parameters that depend on effective anisotropy as a function of magnetic field H.

TABLE IV. The α (Eq. (14)), γ (Eq. (19)), and A (Eq. (18)) parameters as a function of the magnetic field at low temperature region for 2-D CrI3 at B = 2/3 (or J = 0.228 meV).

H (T)	0	2	4	5	9
α (T)	28.3	29.1	29.7	29.9	30.7
γ (mJ/mol K^2)	10.9	9.1	6.7	0.3	0.1
A (mJ/mol $K^{5/2}$)	7.3	3.6	0.5	0.1	0.2

V. SUMMARY

Low dimensional magnetic systems have been studied thoroughly by many scientists recently[4,13,29-32]. Despite these recent efforts, the question of whether the magnetic ordering of many of these materials, including CrI_3, is 2-D or 3-D in nature is as of yet unresolved. From our study, it appears that magnetic and phonon contributions to the specific heat capacity are the most significant contributions in both dimensions. However, the 2-D model for lattice (phonon) contribution (Eq. (11)) to the specific heat capacity, shows (Fig.7) that the magnetic contribution calculated from Eq. (21) is comparable to the lattice contribution in entire range of temperatures in contrast to the 3-D model for lattice contribution (Eq.(5)), where in the high temperature range the magnetic contribution (Fig.8) based on Eq. (21) goes to zero. The behavior of the 3-D model as far as phonon contribution is concerned leads to the expected dependence of the magnetic specific heat capacity as a function of temperature above the Curie temperature. This leads to the phonon 3-D model as appropriate (Eq. (5)) in order to achieve the correct behavior of the specific heat capacity at high temperatures. In the low-temperature range (i.e. $T< 20$ K), the phonon 3-D model forces a 2-D magnetic contribution described by Eq. (14) not by Eq. (8) to fit the experimental data (see, Fig.10). The main conclusion coming out of this discussion confirms a van der Waals gapped and layered structure of the system. It appears, based on our calculations, that this gap is not an obstacle for the phonon contribution to be 3-D in nature. However, from the point of view of the magnetic contribution to the specific heat capacity, the gap creates enough disruptions to maintain a solely-2-D contribution, at least in the low temperature region.

The most important physical property of the magnetic material CrI_3 determined from our comparison of the theoretical and experimental data is the Debye temperature θ_D. Table V summarizes the Debye temperatures for different models including parameter β, and there is a clear discrepancy within the models. The linearization method (Eqs. 18 and 19) gives a Debye temperature of approximately 129 K while the integral method (Eq.5) gives a Debye temperature of 245 K. The latter value can change when during a process of comparing experimental data to phonon contribution we include in Eq. (3) the longitudinal and transverse propagation velocities instead of v_S or the anharmonic nature of the lattice vibrations at the elevated temperatures above T_C[33].

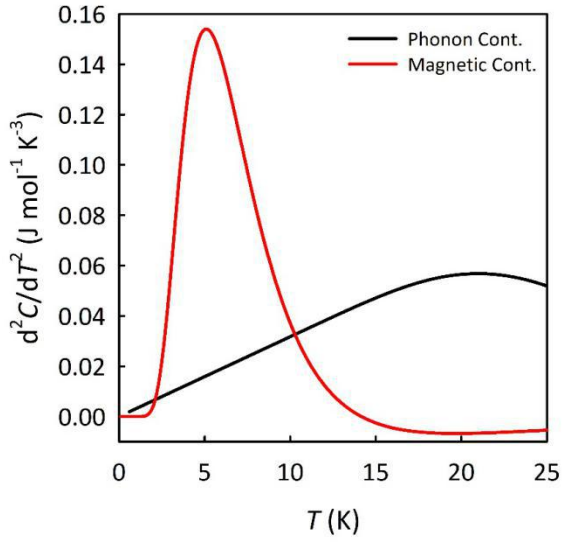

FIG. 11. Second derivative of theoretical phonon contribution (Eq. 5) and the theoretical magnetic contribution (Eq.14) for Θ_D = 245 K and α = 28.32 K between 2 K and 25 K at H = 0 T.

For the linearization method (Eq. 19) to be valid both Eq. (5) and (14) must reduce to Eq. (6) and (17) in the temperature range in which the approximation is made. Fig.11 shows the second derivative of phonon contribution (Eq. 5) is linear until approximately 15 K, which implies that Eq. (6) is only valid between 2 K and 15 K. Eq. (17) is linear and so its second derivative must be zero in its entire range. Fig.11 shows that the magnetic contribution does not approach the derivative of a linear line until after 25 K. With Eqs. (5) and (14) having different temperature ranges in which they are valid there is no temperature range in which the linearization method can be done leaving 245 K to be the Debye temperature which best describes this material.

TABLE V. Average Debye temperatures Θ_D for CrI_3 calculated by using linearization and integral methods for average value of β (see, Eq. (19)).

	β (mJ/mol K)	Θ_D(K)
LINEARIZATION METHOD	3.62	129
INTEGRAL METHOD	-	245

A standard procedure for the estimation of the Debye temperature is based on formula described by Eq. (19) which expresses the specific heat capacity by two terms: the phonon contribution ~ T^3 and the electron contribution ~ T. This is true for a conducting material but in our case, we are dealing with a magnetic semiconductor (CrI_3) which surprisingly contains a linear term according to the spin wave approach (due to magnetism), but at the elevated

temperatures (see Eq. (17)). If we argue that the contribution to specific heat capacity at very low temperatures has a linear term due a weak electronic term (Eq. (19)), the value of Θ_D = 129 K (see, Tab. V) appears to be due to the linearization process of matching values of specific heat capacity described by Eq. (19) and experimental data (Fig. 3a, H = 0 T). This takes place in the very narrow temperature range between 3 K and 6 K. But as we show in Fig. 10, since we have subtracted an optimized phonon contribution (with Θ_D = 245 K) of the specific heat capacity from the experimental data (Eq. (21)), the remaining part of heat capacity matches well with the magnetic properties of CrI_3 described by spin wave model (Eq. (14)). Under these conditions, behaviors of the specific heat capacity as a function of temperature described by Eq. (16), are exponential in nature; when we try to linearize dependence in the form given be Eq. (19), it forces the coefficient γ to be negative (unphysical) between the same range of temperatures (3 K < T < 6 K).

The specific heat capacity of CrI_3 consists of structural (phonon) 3-D contribution and clearly

2-D magnetic contribution. The interesting aspect of our main conclusion is to suggest a measurement of the thermal conductivity in direction which is perpendicular (and parallel) to the layers of CrI_3. The presence of vdW gap between layers in CrI_3 creates a possibility for a rapid heat transfer due to phenomenon called photon tunneling[34] which is created by surface polaritons and/or plasmons. Another very important result of our study is the conclusion that 2-D magnetic properties of CrI_3 requires the presence a very strong anisotropy to maintain off-plane magnetic moments (see Tab.III).

REFERENCES

[1] Y. Liu, L. Wu, X. Tong, J. Li, J. Tao, Y. Zhu, and C. Petrovic, *Scientific Reports*, **9**, 13599 (2019).

[2] C. W. Liu, M. Östling, and J. B. Hannon, *MRS Bull.*, **39**, 658 (2014).

[3] M. C. Lemme, L. J. Li, T. Palacios, and F. Schwierz, *MRS Bull.*, **39**, 711 (2014).

[4] M. A. McGuire, H. Dixit, V. R. Cooper, and B. C. Sales, *Chemistry of Materials*, **27**, 612 (2015). https://doi.org/10.1021/cm504242t.

[5] B. Huang, G. Clark, E. Navarro-Moratalla, D. R. Klein, R. Cheng, K. L. Seyler, D. Zhong, E. Schmidgall, M. A. McGuire, D. H. Cobden, W. Yao, D. Xiao, P. Jarillo-Herrero, and X. Xu, *Nature*, **546**, 270 (2017).

[6] C. Felser, G. H. Fecher, and B. Balke, *Angew. Chem., Int. Ed*., **46**, 668 (2007).

[7] L. L. Handy and N. W. Gregory, *J. Am. Chem. Soc.*, **74**, 891 (1952).

[8] B. Morosin and A. J. Narath, *Chem. Phys.*, **40**, 1958 (1964).

[9] I. Pollini, *Solid State Commun*., **106**, 549 (1998).

[10] W. N. J. Hansen, *Appl. Phys*., **30**, 304S (1959).

[11] W. N. J. Hansen and M. J. Griffel, *Chem. Phys*., **30**, 913 (1959).

[12] J. F. Dillon, Jr. and C. E. J. Olson, *Appl. Phys*., **36**, 1259 (1965).

[13] M. O. Kostryukova and L. V. Luk'yanova, *JETP Letters*, **17**, 54 (1973).

[14] J. L. Lado and J. Fernández-Rossier, *2D Materials*, **4**, 035002 (2017). https://doi.org/10.1088/2053-1583/aa75ed.

[15] G. T. Lin, X. Luo, F. C. Chen, J. Yan, J. J. Gao, Y. Sun, W. Tong, P. Tong, W. J. Lu, Z. G. Sheng, W. H .Song, X. B. Zhu, and Y.P. Sun, *Applied Physics Letters*, **112**, 072405 (2018). https://doi.org/10.1063/1.5019286.

[16] A. Arrott and J. E. Noakes, *Phys. Rev. Lett*., **19**, 786 (1967).

[17] J. S. Kouvel and M. E. Fisher, *Phys. Rev.,* **136**, A1626 (1964).

[18] A. Oleaga, A. Salazar, D. Prabhakaran, J. G. Cheng, and J. S. Zhou, *Phys. Rev*., B **85**, 184425 (2012).

[19] J. Liu, Q. Sun, Y. Kawazoe, and P. Jena, *Phys. Chem. Chem. Phys.,* **18**, 8777 (2016).

[20] W. B. Zhang, Q. Qu, P. Zhu, and C. H. Lam, *J. Mater. Chem.* C **3**, 12457 (2015).

[21] M. A. McGuire, G. Clark, S. Kc, W. M. Chance, G. E. Jellison, V. R. Cooper, X. Xu, and B. C. Sales, *Phys. Rev. Mater.*, **1**, 014001 (2017).

[22] J. J. F. Dillon, *J. Phys. Soc. Jpn.,* **19**, 1662 (1964).

[23] D. Shcherbakov, P. Stepanov, D. Weber,Y. Wang, J. Hu, Y. Zhu, K. Watanabe, T. Taniguchi, Z. Mao, W. Windl, J. Goldberger, M. Bockrath, and C. N. Lau, *Nano Letters*, **18**, 4214 (2018).

[24] C. Kittel, *Introduction to Solid State Physics* (Wiley, New York, 1956) p.435.

[25] J. S. Galsin, *Solid State Physics: An Introduction to Theory* (Academic Press, an imprint of Elsevier, London, 2019) p.160.

[26] A. Narath, *Physical Review*, **131**, 1929 (1963). https://doi.org/10.1103/PhysRev.131.1929.

[27] I. Grosu and M. Crisan, *Journal of Superconductivity and Novel Magnetism*, **33**, 1073 (2019). https://doi.org/10.1007/s10948-019-05320-4.

[28] G. Garton, M. J. M. Leask, W. P. Wolf, and A. F. G. Wyatt, *Journal of Applied Physics,* **34**, 1083 (1963).

[29] L. Chen, J. H. Chung, B. Gao, T. Chen, M. B. Stone, A. I. Kolesnikov, Q. Huang, and P. Dai, *Physical Review X*, **8**, 041028 (2018). https://doi.org/10.1103/PhysRevX.8.041028.

[30] V. M. Bermudez and D. S. McClure, *Journal of Physics and Chemistry of Solids*, **40**, 129 (1979). https://doi.org/10.1016/0022-3697(79)90030-1.

[31] Y. Liu and C. Petrovic, *Physical Review B*, **97**, 174418 (2018). https://doi.org/10.1103/PhysRevB.97.174418.

[32] M. O. Kostryukova, *JETP Letters*, **8**, 141 (1968).

[33] W. Pepperhoff and M. Acet, *Constitution and Magnetism of Iron and its Alloys* (Springer-Verlag, Berlin, Heidelberg, New York, 2015) p.60.

[34] B. Rogers, J. Adams, and S. Pennathur, *Nanotechnology. Understanding Small Systems* (CRC Press, Taylor & Francis Group, Boca Raton, 2001) p.251.